Cell Reports, Volume ■ ■

Supplemental information

NGFR regulates stromal cell activation in germinal centers

Alberto Hernández-Barranco, Vanesa Santos, Marina S. Mazariegos, Eduardo Caleiras, Laura Nogués, Frédéric Mourcin, Simon Léonard, Christelle Oblet, Steve Genebrier, Delphine Rossille, Alberto Benguría, Alba Sanz, Enrique Vázquez, Ana Dopazo, Alejo Efeyan, Ana Ortega-Molina, Michel Cogne, Karin Tarte, and Héctor Peinado

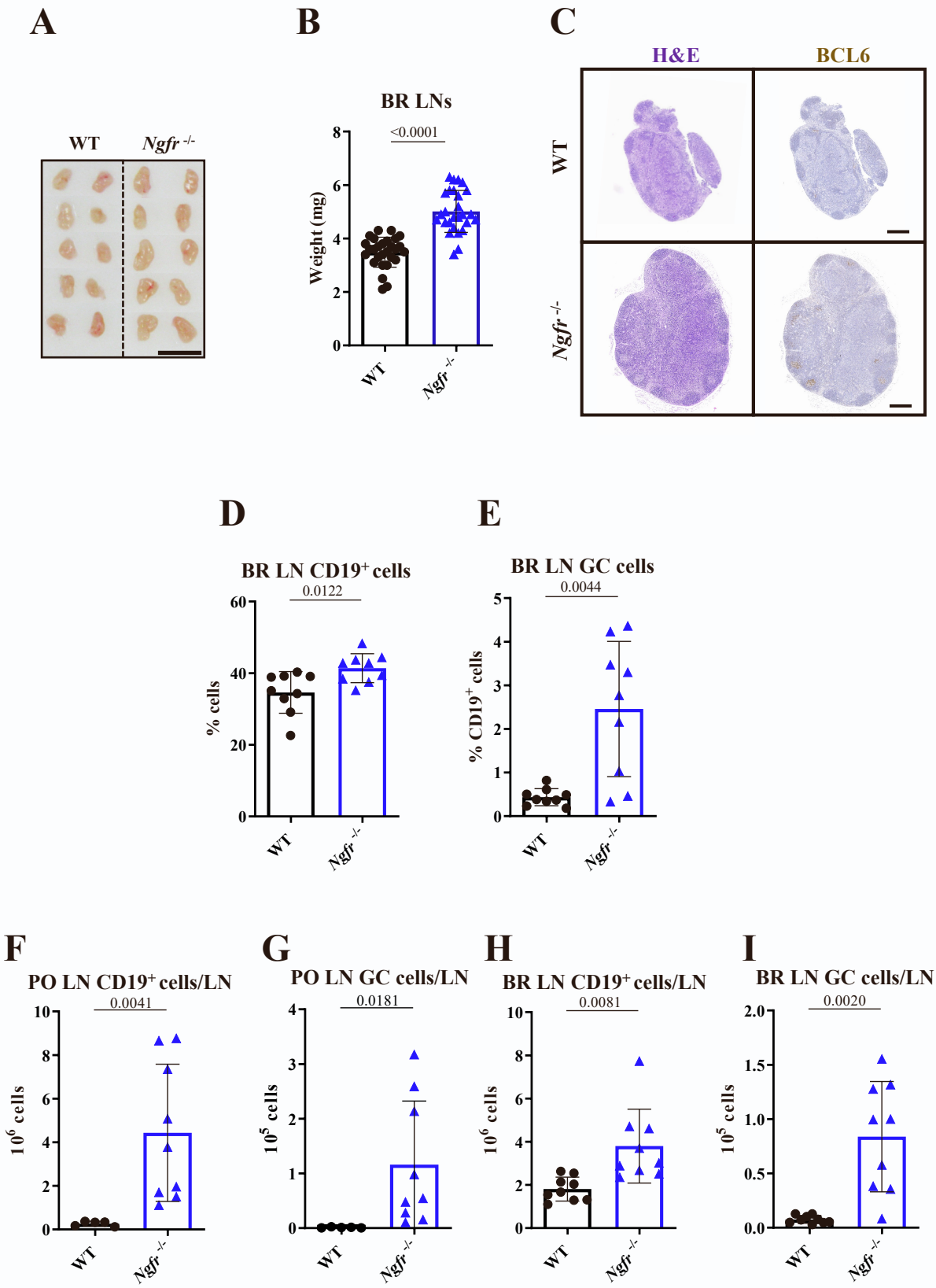
A
WT
Ngfr -/-
B
BR LNs
<0.0001
Weight (mg)
8
6
4
2
0
WT
Ngfr -/-
C
H&E
BCL6
WT
Ngfr -/-
D
BR LN CD19+ cells
0.0122
% cells
60
40
20
0
WT
Ngfr -/-
E
BR LN GC cells
0.0044
% CD19+ cells
5
4
3
2
1
0
WT
Ngfr -/-
F
PO LN CD19+ cells/LN
0.0041
10^6 cells
10
8
6
4
2
0
WT
Ngfr -/-
G
PO LN GC cells/LN
0.0181
10^5 cells
4
3
2
1
0
WT
Ngfr -/-
H
BR LN CD19+ cells/LN
0.0081
10^6 cells
10
8
6
4
2
0
WT
Ngfr -/-
I
BR LN GC cells/LN
0.0020
10^5 cells
2.0
1.5
1.0
0.5
0.0
WT
Ngfr -/-

Figure S1

Figure S1: GC formation in BR LNs

Related to **Figure 2**

A) Representative brachial (BR) LN size in WT and *Ngfr* $^{-/-}$ mice. Scale bar 5mm. **B**) BR LN weight in WT and *Ngfr* $^{-/-}$ mice (n=28 from 3 independent experiments). **C**) Representative H&E and BCL6 immunohistochemistry in BR LNs from WT (upper panels) and *Ngfr* $^{-/-}$ (lower panels) mice. Scale bar, 400µm. **D**) BR LN CD19^{+} cells in WT and *Ngfr* $^{-/-}$ mice (n=9 from 2 independent experiments). **E**) BR LN GC cells in WT and *Ngfr* $^{-/-}$ mice (n=9 from 2 independent experiments). **F**) PO LN CD19^{+} cells/LN in WT and *Ngfr* $^{-/-}$ mice (n=5 from 1 experiment for WT and n=9 from 2 independent experiments for *Ngfr* $^{-/-}$ mice). **G**) PO LN GC cells/LN in WT and *Ngfr* $^{-/-}$ mice (n=5 from 1 experiment for WT and n=9 from 2 independent experiments for *Ngfr* $^{-/-}$ mice). **H**) BR LN CD19^{+} cells/LN in WT and *Ngfr* $^{-/-}$ mice (n=9 from 2 independent experiments). **I**) BR LN GC cells/LN in WT and *Ngfr* $^{-/-}$ mice (n=9 from 2 independent experiments). The graphs in **B**, **D, E, F, G, H** and **I** show the mean and SD error bars and the P-values by a two-tailed unpaired t-test with Welch's correction.

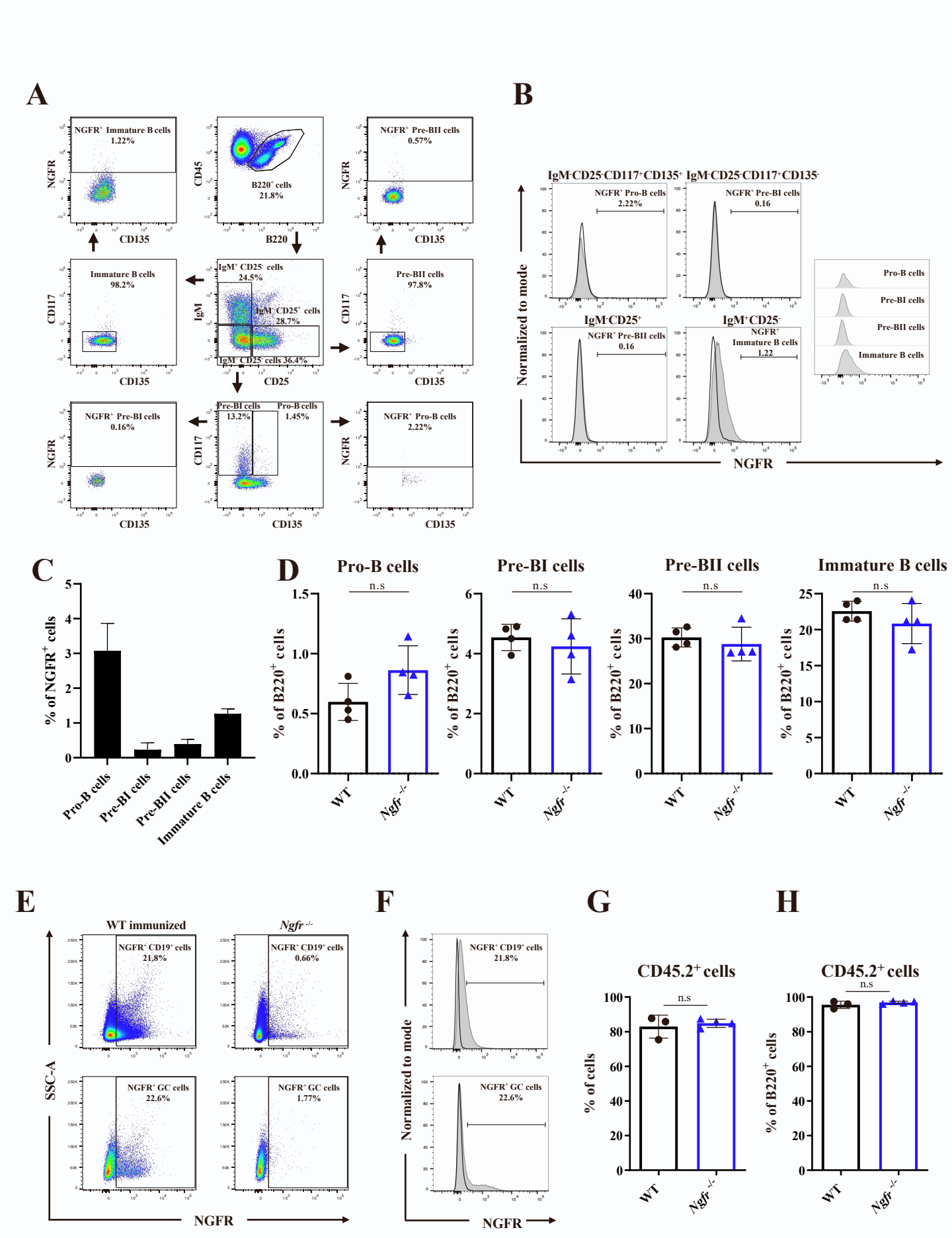
A
NGFR+ Immature B cells 1.22%
B220+ cells 21.8%
NGFR+ Pre-BII cells 0.57%
Immature B cells 98.2%
IgM+ CD25- cells 24.5%
IgM- CD25+ cells 28.7%
IgM- CD25- cells 36.4%
Pre-BII cells 97.8%
NGFR+ Pre-BI cells 0.16%
Pre-BI cells 13.2%
Pro-B cells 1.45%
NGFR+ Pro-B cells 2.22%
CD135
B220
CD25
CD45
NGFR
CD117
IgM
B
IgM-CD25-CD117+CD135+
IgM-CD25-CD117+CD135-
NGFR+ Pro-B cells 2.22%
NGFR+ Pre-BI cells 0.16
IgM-CD25+
IgM+CD25-
NGFR+ Pre-BII cells 0.16
NGFR+ Immature B cells 1.22
Pro-B cells
Pre-BI cells
Pre-BII cells
Immature B cells
Normalized to mode
NGFR
C
% of NGFR+ cells
Pro-B cells
Pre-BI cells
Pre-BII cells
Immature B cells
D
Pro-B cells
Pre-BI cells
Pre-BII cells
Immature B cells
n.s
% of B220+ cells
WT
Ngfr -/-
E
WT immunized
Ngfr -/-
NGFR+ CD19+ cells 21.8%
NGFR+ CD19+ cells 0.66%
NGFR+ GC cells 22.6%
NGFR+ GC cells 1.77%
SSC-A
NGFR
F
NGFR+ CD19+ cells 21.8%
NGFR+ GC cells 22.6%
Normalized to mode
NGFR
G
CD45.2+ cells
n.s
% of cells
WT
Ngfr -/-
H
CD45.2+ cells
n.s
% of B220+ cells
WT
Ngfr -/-

Figure S2

Figure S2: Analysis of NGFR expression in immune cells

Related to **Figure 3**

A) Gating strategy to study NGFR expression by B cell precursors in the BM. **B**) Histograms comparing mean NGFR fluorescence in BM B cell precursors from the WT mice gated in **A**. The black lines represent the NGFR fluorescence in *Ngfr*$^{-/-}$ BM cells as a negative control. **C**) The proportion of NGFR^{+} cells among BM B cell precursors. **D**) Frequencies of the different BM B cell precursor populations in WT and *Ngfr*$^{-/-}$ mice (n=4 from 1 experiment). **E**) Representative plots of NGFR expression in the CD19^{+} and the CD19^{+}CD95^{+}CD38^{lo} GC B cells subsets in WT and *Ngfr*$^{-/-}$ LNs assessed by flow cytometry. **F**) Histograms comparing the mean NGFR fluorescence in the populations gated in **E**. The black lines represent NGFR fluorescence in *Ngfr*$^{-/-}$ mice used as a negative control. **G**) Flow cytometry quantification of the proportion of CD45.2^{+} total cells in the blood of CD45.1 BM reconstituted mice (n=3 WT and 4 *Ngfr*$^{-/-}$ CD45.2 BM donors from 1 experiment). **H**) Flow cytometry quantification of the proportion of CD45.2^{+} B220^{+} cells in the blood of CD45.1 BM reconstituted mice (n=3 WT and 4 *Ngfr*$^{-/-}$ CD45.2 BM donors from 1 experiment). Graphs in **D**, **G and H** shows the mean and SD error bars, and the P-values by two-tailed unpaired t-test with Welch's correction (except for pre-BII cells in panel **D**, which was calculated with a two-tailed Mann-Whitney test).

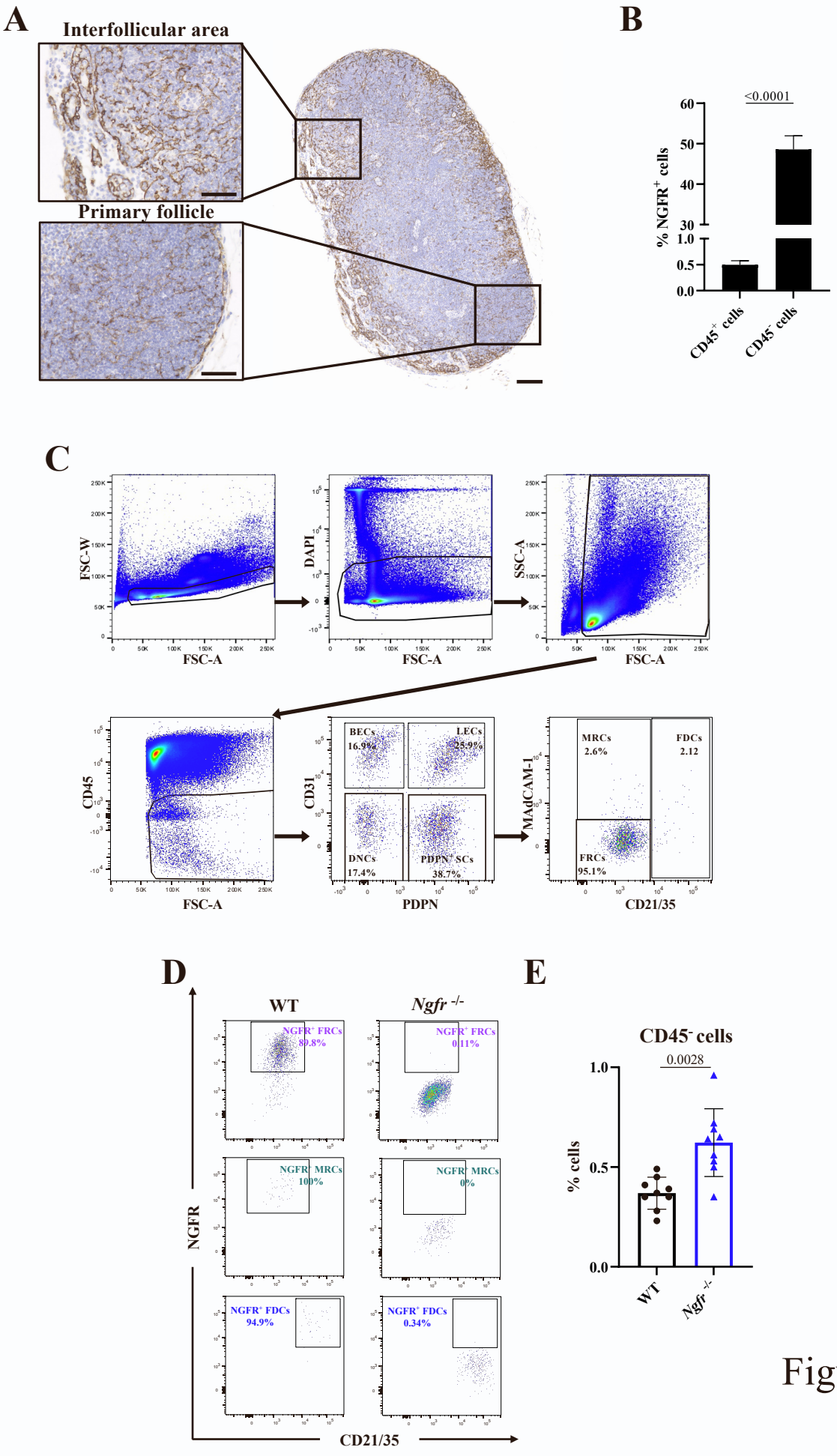
A
Interfollicular area
Primary follicle
B
<0.0001
% NGFR+ cells
CD45+ cells
CD45- cells
C
FSC-W
FSC-A
DAPI
SSC-A
CD45
CD31
PDPN
MAdCAM-1
CD21/35
BECs 16.9%
LECs 25.9%
DNCs 17.4%
PDPN- SCs 38.7%
MRCs 2.6%
FDCs 2.12
FRCs 95.1%
D
WT
Ngfr -/-
NGFR
CD21/35
NGFR+ FRCs 89.8%
NGFR+ FRCs 0.11%
NGFR- MRCs 100%
NGFR- MRCs 0%
NGFR+ FDCs 94.9%
NGFR+ FDCs 0.34%
E
CD45- cells
0.0028
% cells
WT
Ngfr -/-

Figure S3

Figure S3: Analysis of NGFR expression in LN stromal cells

Related to **Figure 3**

A) Representative NGFR IHC in the PO LN showing the whole architecture of the organ (scale bar, 100 µm) and a magnification of different substructures (scale bar, 50 µm). **B**) Flow cytometry quantification of the proportion of $NGFR^+$ cells in the immune ($CD45^+$) and stromal ($CD45^-$) cell populations of PO LNs (n=9 from 2 independent experiments). **C**) Gating strategy of $CD45^-$ LN stromal populations. **D**) Representative plots of NGFR expression in the $PDPN^+$ SC subsets in WT and *Ngfr* $^{-/-}$ LNs. **E**) Relative $CD45^+$ and $CD45^-$ cell populations expressing NGFR in *Ngfr* WT PO LNs (n=9 from 2 independent experiments). The graphs in **B and E** show the mean and SD error bars, and the P-values by a two-tailed unpaired t-test with Welch's correction .

Table S2: GSEA in Reactome of the differentially expressed genes in WT and *Ngfr* $^{-/-}$ FDCs

Related to Figure 4

The gene sets were obtained by GSEA of the differentially expressed genes in *Ngfr* $^{-/-}$ vs WT FDCs Table S1). Settings were established for 1,000 gene set permutations. Only those gene sets with more than 20 genes were finally considered.

Positively enriched Reactome gene sets in *Ngfr* $^{-/-}$ and WT FDCs								
Reactome gene set	**SIZE**	**ES**	**NES**	**NOM p-val**	**FDR q-val**	**FWER p-val**	**RANK AT MAX**	**LEADING EDGE**
REACTOME_ADAPTIVE_IMMUNE_SYSTEM	24	0.45	2.21	0.002	0.009	0.009	54	tags=46%, list=13%, signal=50%
REACTOME_HEMOSTASIS	33	0.34	1.81	0.012	0.086	0.134	118	tags=52%, list=28%, signal=66%
REACTOME_METABOLISM_OF_LIPIDS	40	0.28	1.64	0.035	0.145	0.313	260	tags=90%, list=61%, signal=211%
REACTOME_CYTOKINE_SIGNALING_IN_IMMUNE_SYSTEM	23	0.32	1.53	0.077	0.189	0.485	146	tags=57%, list=34%, signal=82%
REACTOME_MEMBRANE_TRAFFICKING	25	0.30	1.43	0.094	0.235	0.647	71	tags=36%, list=17%, signal=41%
REACTOME_NEUTROPHIL_DEGRANULATION	25	0.29	1.40	0.111	0.227	0.693	122	tags=48%, list=29%, signal=63%
REACTOME_VESICLE_MEDIATED_TRANSPORT	27	0.27	1.36	0.156	0.232	0.759	54	tags=30%, list=13%, signal=32%
REACTOME_POST_TRANSLATIONAL_PROTEIN_MODIFICATION	42	0.23	1.34	0.142	0.221	0.783	58	tags=26%, list=14%, signal=27%
REACTOME_INNATE_IMMUNE_SYSTEM	44	0.22	1.26	0.209	0.271	0.872	259	tags=80%, list=61%, signal=183%
REACTOME_INFECTIOUS_DISEASE	25	0.21	1.00	0.458	0.544	0.990	145	tags=48%, list=34%, signal=69%
REACTOME_SIGNALING_BY_GPCR	22	0.19	0.90	0.584	0.629	0.999	74	tags=27%, list=17%, signal=31%
REACTOME_NERVOUS_SYSTEM_DEVELOPMENT	25	0.16	0.77	0.779	0.748	1.000	138	tags=40%, list=33%, signal=56%

Negatively enriched Reactome gene sets in *Ngfr* $^{-/-}$ and WT FDCs								
Reactome gene set	**SIZE**	**ES**	**NES**	**NOM p-val**	**FDR q-val**	**FWER p-val**	**RANK AT MAX**	**LEADING EDGE**
REACTOME_RNA_POLYMERASE_II_TRANSCRIPTION	22	-0.35	-1.84	0.022	0.041	0.068	159	tags=73%, list=38%, signal=110%
REACTOME_DEVELOPMENTAL_BIOLOGY	31	-0.19	-1.15	0.261	0.406	0.766	140	tags=52%, list=33%, signal=71%
REACTOME_SIGNALING_BY_RHO_GTPASES_MIRO_GTPASES_AND_RHOBTB3	22	-0.19	-0.98	0.497	0.467	0.918	197	tags=73%, list=46%, signal=129%

ES (Enrichment Score)

NES (Normalized Enrichment Score)

FDR q-val (False Discovery Rate q-value)

FWER p-val (Family-Wise Error Rate p-value)

RANK AT MAX (Rank at Maximum)

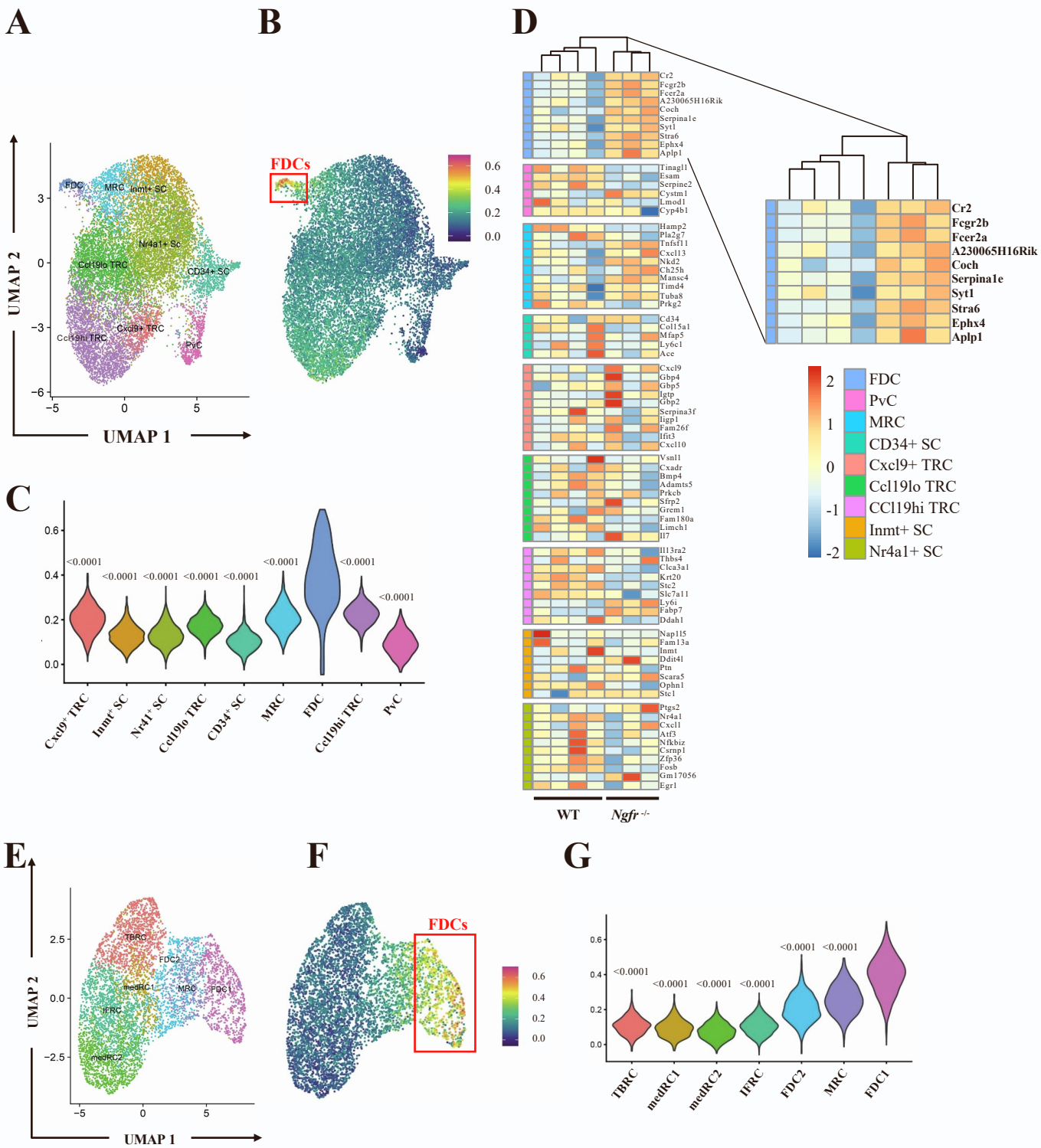
A
B
C
D
E
F
G
FDC
MRC
Inmt+ SC
Nr4a1+ Sc
Ccl19lo TRC
CD34+ SC
Cxcl9+ TRC
Ccl19hi TRC
PvC
UMAP 1
UMAP 2
FDCs
Cxcl9+ TRC
Inmt+ SC
Nr41+ SC
Ccl19lo TRC
CD34+ SC
MRC
FDC
Ccl19hi TRC
PvC
<0.0001
WT
Ngfr -/-
FDC
PvC
MRC
CD34+ SC
Cxcl9+ TRC
Ccl19lo TRC
CCl19hi TRC
Inmt+ SC
Nr4a1+ SC
TBRC
FDC2
medRC1
MRC
FDC1
IFRC
medRC2

Figure S4

Figure S4: Analysis of FDC activation signatures in scRNAseq datasets

Related to **Figure 4**

A) UMAP plot showing the distribution of the different subsets of stromal cells previously identified by scRNAseq by Rodda LB et al.[1] **B**) Heat map comparing the up-regulated gene signature in FDCs obtained from the *Ngfr* $^{-/-}$ and WT mice, with the clusters shown in **A**. **C**) Violin plots showing the relative identity of the up-regulated signature in the different cell subsets defined in **A**. The statistics refer to the comparison of each population with the FDC subset. **D**) Heat map showing the differential expression derived from the RNAseq analysis of FDCs from *Ngfr* $^{-/-}$ and WT mice for the top 10 genes defining each subset found previously by Rodda LB et al.[1] and a magnification of the FDC cluster. The color code identifies each population according to the UMAP distribution in **A**. **E**) UMAP plot showing the distribution of the different subsets of stromal cells previously identified by scRNAseq by Pikor NB et al.[2] **F**) Heat map comparing the up-regulated gene signature in FDCs of *Ngfr* $^{-/-}$ and WT mice with the clusters shown in **E**. **G**) Violin plots showing the relative identity of the up-regulated signature in the different cell subsets identified in **E**. The statistics refer to the comparison of each population with the FDC1 subset. The P-values by a two-tailed unpaired T-test with Welch's correction in **C and G**.

Table S3: Differentially expressed genes between immunized and naïve FDCs identified by Pikor NB et al

Related to Figure 4

The signatures were obtained from the immunized and non-immunized conditions within the FDC1 cluster (Pikor et al., 2020), computed with the FindMarkers function from the Seurat R package using Wilcoxon test (with the following parameters: avg_log2FC>0.25 or <-0.25 and p_val_adj<0.05)

Immunized FDC1 significant up-regulated genes	Immunized FDC1 significant down-regulated genes
Coch	Rpl37
Fcer2a	Alyref
Epcam	mt-Co3
Postn	Gm48565
Serpine1	Tmed2
S100a10	Rps25
Igkc	Phpt1
Tmem119	Gm8624
Serpinb1a	Gm10177
Plpp3	Ost4
Gm8730	mt-Atp8
Mpz	Gfra2
Blnk	Tcf7l2
Fcgr2b	Rpl13
Anxa2	Rpl36
AI987944	Rpl13a
Pvalb	C1s1
Tuba1a	Dsc3
Tnfrsf9	Il6st
Ubd	Usp50
Art2a-ps	Fads1
Dio1	Bloc1s1
Stmn2	Cox7c
Klf6	Pdia4
Tmem37	Aif1
Cdc42ep3	Tsix
Chka	Ltbp2
Cyba	Rps16
Tmsb4x	Irf2bp2
Prnp	Rpl37rt
Castor2	Ubb
Apobec3	Fdft1
Lpcat1	Tmem258
H2-M2	Grcc10
Traf1	Gpx1
Irf8	Myl12b
Plppr1	Cox17
Il4i1	Rpl24
Homer2	Scd2
Pon2	Gm1821
Pnisr	Ndufa3
Pthlh	Gpx4-ps2
S100a4	Cebpb
Actb	Cd302

Table S3 part 2

Immunized FDC1 significant up-regulated genes	Immunized FDC1 significant down-regulated genes
Aplp1	Nme2
Ighg1	Tomm7
Map1b	Rpl37a
Crip1	Rps29
Gdi1	Rpl41
Serpinb8	Serpina1b
Lxn	Rpl36a
Vsig10	Sulf1
Tesc	Serf2
Ttc14	Gm11478
Tcim	Rps21
Pwwp2a	Rps27
Agpat4	Rpl15
Zfp871	Rpl38
Abhd18	Rps6
Aif1l	Gm12216
Nrp2	Ftl1-ps1
Anxa5	Fth1
Lrrk1	Rbp1
Syngr2	Gm36899
Ctsh	Serpina12
Kif5b	Rpl27a
Nacc2	Rpl36al
Ceacam15	Uba52
Rasa2	Fdps
Hoxc9	C4b
Epha4	Rpl27
Nfkbia	Ifitm3
Pbxip1	Rps27rt
Trak1	Gm11808
Slc16a6	Ndufb4
Actg1	Rnaset2a
Iscu	Rpl10-ps3
Dapk2	Rpl35a
Trim12a	Rps10
Gdap10	mt-Atp6
Vcam1	Mt2
Hoxc10	Id2
Fam214b	Cfb
Eif2s3y	Cxcl13
	Atp5l
	Snrpg
	Rnaset2b
	Mt1
	Id3
	Rps28

Table S4: Curated list of relevant genes in FDC biology

Related to Figure 4

Gene	Reference	Functional subgroup
Cr2	**15,27,48,50,52,53**	Complement and Fc receptors
Fcamr	**27**	
Fcer2a	**15,27,52**	
Fcgr2b	**15,27,48**	
Coch	**15,27**	Cell stiffness, dendritic shape
Homer2	**27**	
Postn	**27**	
Tmem119	**27**	
Myh11	**27**	
Vcam1	**15,50,51**	Adhesion molecules
Icam1	**15,49,50,51**	
Madcam1	**15,27,50**	
Cxcl13	**15,27,48,53**	Chemotactic factors
Ccl19	**27**	
Ggt5	**53**	
Spns2	**53**	
Tnfsf13b	**15,27,48**	Survival factors, interleukins and their receptors
Il7	**27**	
Il15	**55**	
Il4ra	**52**	
Mfge8	**15,47**	B and T cell regulators
Tnfrsf9	**47**	
Cd40	**15**	
Cd200	**56**	
Prnp	**15**	Other molecules
Pthlh	**27**	
Sox9	**27,53**	

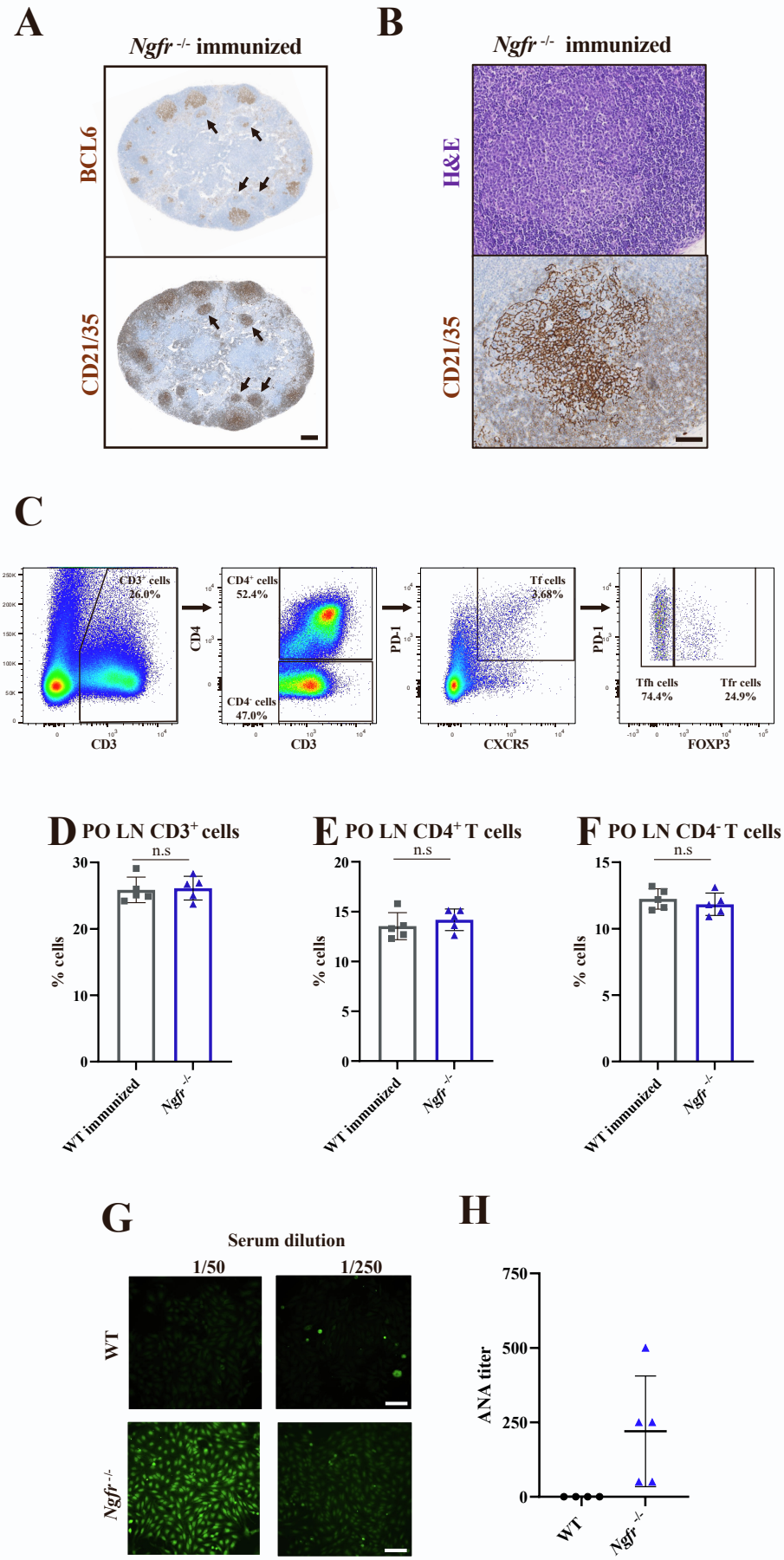
A
Ngfr -/- immunized
BCL6
CD21/35
B
Ngfr -/- immunized
H&E
CD21/35
C
CD3+ cells
26.0%
SSC-A
CD3
CD4+ cells
52.4%
CD4- cells
47.0%
CD4
CD3
Tf cells
3.68%
PD-1
CXCR5
Tfh cells
74.4%
Tfr cells
24.9%
PD-1
FOXP3
D PO LN CD3+ cells
n.s
% cells
WT immunized
Ngfr -/-
E PO LN CD4+ T cells
n.s
% cells
WT immunized
Ngfr -/-
F PO LN CD4- T cells
n.s
% cells
WT immunized
Ngfr -/-
G
Serum dilution
1/50
1/250
WT
Ngfr -/-
H
ANA titer
WT
Ngfr -/-

Figure S5

Figure S5: Characterization of T follicular cells and ANA production in *Ngfr* $^{-/-}$ mice

Related to **Figure 5 and 6**

A) Representative images of BCL6 and CD21/35 staining in PO LNs from *Ngfr* $^{-/-}$ immunized mice. The black arrows indicate the formation of misplaced GCs. Scale bar, 200µm. **B**) Representative H&E image (upper panel) and CD21/35 staining (lower panel) in GCs from *Ngfr* $^{-/-}$ immunized PO LNs. Scale bar, 50 µm. **C**) Gating strategy used in the flow cytometry analysis of LN T cells, including T follicular (Tf) cells. **D**) Flow cytometry quantification of the total T cells ($CD3^{+}$) in WT immunized and *Ngfr* $^{-/-}$ PO LNs. **E**) Flow cytometry quantification of the $CD4^{+}$ T cells in WT immunized and *Ngfr* $^{-/-}$ PO LNs. **F**) Flow cytometry quantification of the $CD4^{-}$ T cells in WT immunized and *Ngfr* $^{-/-}$ PO LNs (n=5 from 1 experiment in **D**, **E and F**). **G**) Representative IHF images of Hep-2 cells slides incubated with sera from 10-week-old WT and *Ngfr* $^{-/-}$ mice at the dilutions indicated. Scale bar, 100µm. **H**) Semi-quantitative measurement of the ANA titers in WT and *Ngfr* $^{-/-}$ mice sera (n=4 WT and n=5 *Ngfr* $^{-/-}$ mice). The graphs in **D**, **E and F** show the mean and SD error bars and the P-values by a two-tailed unpaired t-test and Welch's correction. The statistical analysis in **H** is not show as all the values in the WT sera were 0.

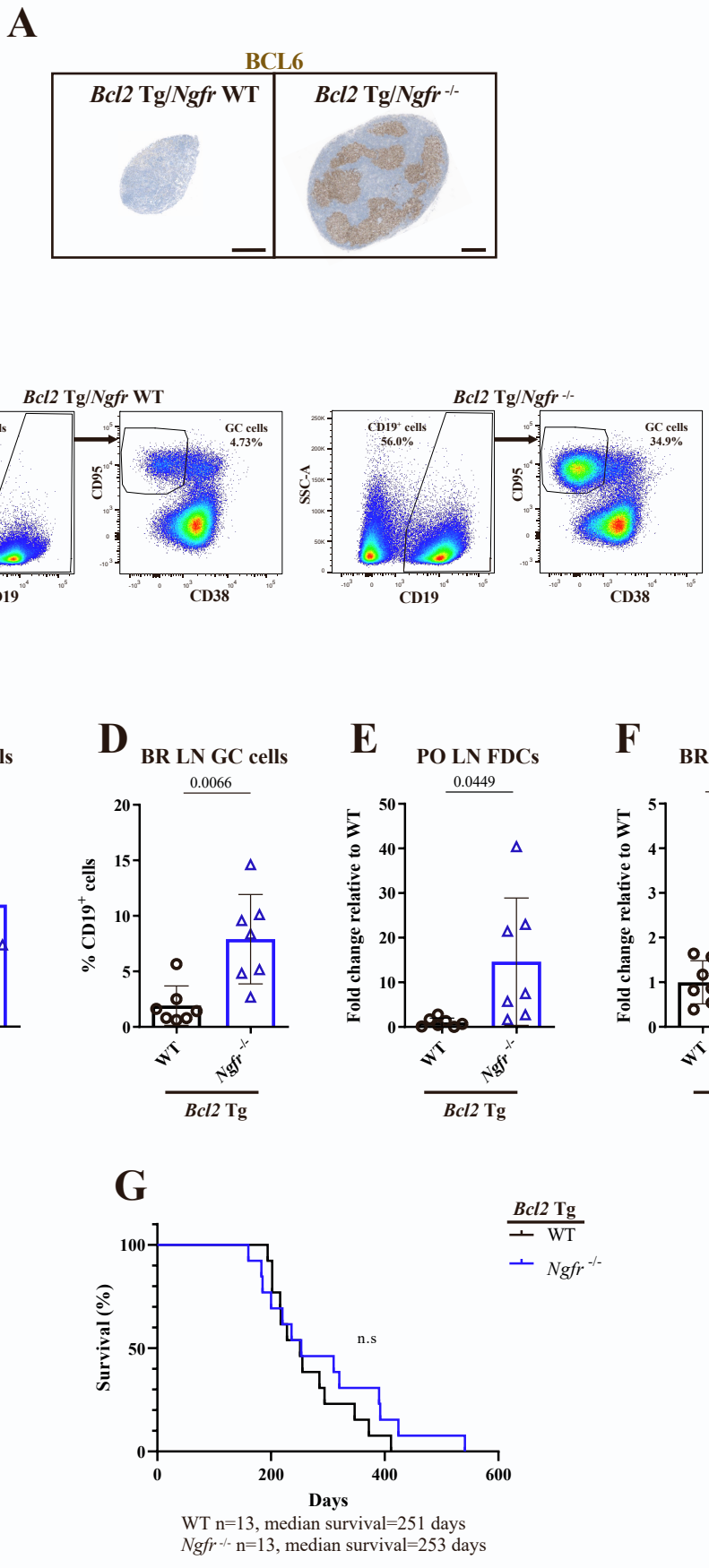
A
BCL6
Bcl2 Tg/Ngfr WT
Bcl2 Tg/Ngfr -/-
B
Bcl2 Tg/Ngfr WT
CD19+ cells
41.1%
GC cells
4.73%
SSC-A
CD19
CD95
CD38
Bcl2 Tg/Ngfr -/-
CD19+ cells
56.0%
GC cells
34.9%
C
PO LN GC cells
0.0023
% CD19+ cells
WT
Ngfr -/-
Bcl2 Tg
D
BR LN GC cells
0.0066
% CD19+ cells
E
PO LN FDCs
0.0449
Fold change relative to WT
F
BR LN FDCs
0.0005
Fold change relative to WT
G
Bcl2 Tg
WT
Ngfr -/-
Survival (%)
n.s
Days
WT n=13, median survival=251 days
Ngfr -/- n=13, median survival=253 days

Figure 6

Figure S6: Characterization of GC formation in the *Bcl2* Tg/*Ngfr* $^{-/-}$ model

Related to **Figure 6**

A) Representative images of BCL6 IHC in PO LN from 10-week-old *Bcl2* Tg crossed with *Ngfr* WT or *Ngfr* $^{-/-}$ mice. Scale bar, 400µm. **B**) Representative examples of the gating strategy for CD19^{+} and GC cells in PO LN from *Bcl2* Tg/*Ngfr* WT (left panels) and *Bcl2* Tg/*Ngfr* $^{-/-}$ (right panels) mice. **C**) Flow cytometry quantification of PO LN GC cells in *Bcl2* Tg/*Ngfr* WT and *Bcl2* Tg/*Ngfr* $^{-/-}$ mice (n=7 for *Bcl2* Tg/*Ngfr* WT and n=6 for *Bcl2* Tg/*Ngfr* $^{-/-}$ mice from 2 independent experiments). **D**) Flow cytometry quantification of BR LN GC cells in *Bcl2* Tg/*Ngfr* WT and *Bcl2* Tg/*Ngfr* $^{-/-}$ mice (n=7 for *Bcl2* Tg/*Ngfr* WT and *Bcl2* Tg/*Ngfr* $^{-/-}$ mice from 2 independent experiments). **E**) Flow cytometry quantification of PO LN FDCs in *Bcl2* Tg/*Ngfr* WT and *Bcl2* Tg/*Ngfr* $^{-/-}$ mice. The total cell frequency is relative to the *Bcl2* Tg/*Ngfr* WT values and expressed as the fold change (n=7 for *Bcl2* Tg/*Ngfr* WT and *Bcl2* Tg/*Ngfr* $^{-/-}$ mice from 2 independent experiments). **F**) Flow cytometry quantification of BR LN FDCs in *Bcl2* Tg/*Ngfr* WT and *Bcl2* Tg/*Ngfr* $^{-/-}$ mice. The total cell frequency is relative to the *Bcl2* Tg/*Ngfr* WT values and expressed as the fold change (n=7 for *Bcl2* Tg/*Ngfr* WT and *Bcl2* Tg/*Ngfr* $^{-/-}$ mice from 2 independent experiments). **G**) Survival curve of *Bcl2* Tg/*Ngfr* WT and *Bcl2* Tg/*Ngfr* $^{-/-}$ female mice. n=13 *Bcl2* Tg/*Ngfr* WT and n=13 *Bcl2* Tg/*Ngfr* $^{-/-}$). P value by a Log-rank (Mantel-Cox). The graphs in **C**, **D**, **E and F** show the mean and SD error bars and, the P-values by a two-tailed unpaired t-test with Welch's correction.

Supplemental references:

[1] Rodda, L.B., Lu, E., Bennett, M.L., Sokol, C.L., Wang, X., Luther, S.A., Barres, B.A., Luster, A.D., Ye, C.J., and Cyster, J.G. (2018). Single-Cell RNA Sequencing of Lymph Node Stromal Cells Reveals Niche-Associated Heterogeneity. Immunity *48*, 1014-1028 e1016. 10.1016/j.immuni.2018.04.006.

[2] Pikor, N.B., Morbe, U., Lutge, M., Gil-Cruz, C., Perez-Shibayama, C., Novkovic, M., Cheng, H.W., Nombela-Arrieta, C., Nagasawa, T., Linterman, M.A., et al. (2020). Remodeling of light and dark zone follicular dendritic cells governs germinal center responses. Nat Immunol *21*, 649-659. 10.1038/s41590-020-0672-y.